Multiphoton excitation of surface plasmon-polaritons and scaling of nanoripple formation in large bandgap materials

Susanta Kumar Das [1,a], Hamza Messaoudi [1], Abishek Debroy [1], Enda McGlynn[2], and Ruediger Grunwald [1,b]

[1]*Max Born Institute Nonlinear Optics and Short-Pulse Spectroscopy, Max-Born-Strasse 2a, D-12489 Berlin, Germany*

[2]*School of Physical Sciences, National Centre for Plasma Science and Technology, Dublin City University, Glasnevin, Dublin 9, Ireland*

[a]susant2@rediffmail.com

[b]grunwald@mbi-berlin.de

Abstract: We report studies of multiphoton mechanisms of plasmon excitation and their influence on the femtosecond-laser induced sub-wavelength ripple generation in large-bandgap dielectric and semiconducting transparent materials. An extended Drude-Sipe formalism is applied to quantitatively estimate the real part of the dielectric function which is dependent on the carrier density. The theory is able to predict the ripple periods for selected materials in good agreement with the experimental observations. Possible limitations at very small spatial periods are also discussed.

OCIS codes: (220.4241) Nanostructure fabrication; (050.6624) Subwavelength structures; (140.3390) Laser materials processing.

References and links

1. M. Birnbaum, "Semiconductor Surface Damage Produced by Ruby Lasers," J. Appl. Phys. **36**, 3688 (1965).
2. A. Y. Vorobyev and C. Guo, "Effects of nanostructure-covered femtosecond laser-induced periodic surface structures on optical absorptance of metals," Appl. Phys. **A 86**, 321-24 (2007).
3. M. Shen, J. E. Carey, C. H. Crouch, M. Kandyla, H. A. Stone, and E. Mazur, "High-density regular arrays of nanometer-scale rods formed on silicon surfaces via femtosecond laser irradiation in water," Nano Lett. **8**, 2087-2091 (2008).
4. B. Kumar and R. K. Soni, "Submicrometre periodic surface structures in InP induced by nanosecond UV laser pulses," J. Phys. D: Appl. Phys. **41**, 155303 (2008).
5. R. Taylor, C. Hnatovsky, and E. Simova, "Applications of femtosecond laser induced self-organized planar nanocracks inside fused silica glass," Laser & Photon. Rev. **2**, 26-46 (2008).
6. J. Bonse, H. Sturm, H., D. Schmidt, W. Kautek, "Chemical, morphological and accumulation phenomena in ultrashort-pulse laser ablation of TiN in air," Appl. Phys. A **71**, 657-667 (2000).
7. H. Hiraoka, W. Y. Y. Wong, T. M. Wong, C. T. Hung, W. C. Loh, and F. M. Lee, "Pulsed laser processing of polymer and ceramic surfaces," J. Photopolymer Sci. Technol. **10**, 205-210 (1997).
8. S. Baudach, J. Bonse, and W. Kautek, "Ablation experiments on polyimide with femtosecond laser pulses," Appl. Phys. A **69**, S395 (1999).
9. J. E. Sipe, J. F. Young, J. S. Preston, and H. M. van Driel, "Laser induced periodic surface structure. I. Theory," Phys. Rev. **B 27**, 1141 (1983).
10. K. W. Kolasinski, "Solid structure formation during the liquid/solid phase transition," Current Opinion in Solid State and Materials Science **11,** 76-85 (2007).
11. C. H. Lin, L. Jiang, H. Xiao, S. J. Chen, and H. L. Tsai, "Surface-enhanced Raman scattering microchip fabricated by femtosecond laser," Opt. Lett. **35**, 2937-2939 (2010).
12. E. D. Diebold,N. H. Mack, Stephen K. Doorn, and E. Mazur, "Femtosecond laser-nanostructured substrates for surface-enhanced Raman scattering," Langmuir **25**, 1790 (2009).
13. C. H. Lin, L. Jiang, Y. H. Chai, H. Xiao, S. J. Chen, and H. L. Tsai, "One-step fabrication of nanostructures by femtosecond laser for surface-enhanced Raman scattering," Opt. Express **17**, 21581 (2009).
14. A. Y. Vorobyev and C. Guoa, Colorizing metals with femtosecond laser pulses, Appl. Phys. Lett. **92**, 041914 (2008).
15. B. Dusser, Z. Sagan, H. Soder, N. Faure, J. P. Colombier, M. Jourlin and E. Audouard, "Controlled nanostructrures formation by ultra fast laser pulses for color marking," Opt Express. **18**, 2913 (2010).
16. A.Y. Vorobyev, V. S. Makin, and Chunlei Guo, "Brighter light sources from black metal: significant

increase in emission efficiency of incandescent light sources," Phys. Rev. Lett. **102**, 234301 (2009).
17. J. Eichstädt, G. R. B. E. Römer, and A.J. Huis in't Veld, "Towards friction control using laser-induced periodic surface structures," Physics Procedia **12**, 7 (2011).
18. T. Y. Hwang, A. Y. Vorobyev, and C. Guo, "Surface-plasmon-enhanced photoelectron emission from nanostructure-covered periodic grooves on metals," Phys. Rev. B **79**, 085425 (2009).
19. R. Torres, T. E. Itina, V. Vervisch, M. Halbwax, T. Derrien, T. Sarnet, M. Sentis, J. Ferreira, F. Torregrosa, and L. Roux, "Study on laser induced periodic structures and photovoltaic application," AIP Conf. Proc. **1278**, 576 (2010).
20. Y. Shimotsuma, M. Sakakura, K. Miura, J. R. Qiu, P. G. Kazansky, K. Fujita, and K. Hirao, "Application of femtosecond-laser induced nanostructures in optical memory," J. Nanosci. Nanotech. **7**, 94-104 (2007).
21. T. Baldacchini, J. E. Carey, M. Zhou, and E. Mazur, "Superhydrophobic surfaces prepared by microstructuring of silicon using a femtosecond laser," Langmuir **22**, 4917 (2006).
22. J. T. Chen, W. C. Lai, Y. J. Kao, Y. Y. Yang, and J. K. Sheu, "Laser-induced periodic structures for light extraction efficiency enhancement of GaN-based light emitting diodes," Opt. Express **20**, 5689 (2012).
23. W. L. Barnes, "Surface plasmon-polariton length scales: a route to sub-wavelength optics," J. Opt. A: Pure Appl. Opt. **8**, S87-S93 (2006).
24. M. Huang, F. Zhao, Y. Cheng, N. Xu, and Z. Xu, "Mechanisms of ultrafast laser-induced deep-subwavelength gratings on graphite and diamond," Phys. Rev. B **79**, 125436 (2009).
25. Y. Shimotsuma, P. G. Kazansky, J. Qiu, K. Hirao, "Self-organized nanogratings in glass irradiated by ultrashort light pulses," Phys. Rev. Lett. **91**, 47405 (2003).
26. M. Huang, F. Zhao, Y. Cheng, N. Xu, and Z. Xu, "Origin of laser-induced near-subwavelength ripples: interference between surface plasmons and incident laser," ACS Nano **3**, 4062 (2009).
27. J. Bonse, A. Rosenfeld, and J. Krüger, "On the role of surface plasmon polaritons in the formation of laser-induced periodic surface structures upon irradiation of silicon by femtosecond-laser pulses," J. Appl. Phys. **106**, 104910 (2009).
28. F. Garrelie, J. P. Colombier, F. Pigeon, S. Tonchev, N. Faure, M. Bounhalli, S. Reynaud, and O. Parriaux, "Evidence of surface plasmon resonance in ultrafast laser-induced ripples," Opt. Express **19**, 9035 (2011).
29. K. Okamuro, M. Hashida, Y. Miyasaka, Y. Ikuta, S. Tokita, and S. Sakabe, "Laser fluence dependence of periodic grating structures formed on metal surfaces under femtosecond laser pulse irradiation," Phys. Rev. B **82**, 165417 (2010).
30. S. K. Das, F. Guell, H. Messaoudi, M. Bock, and R. Grunwald, "Evidence for non-mass-transfer mechanism in fs-laser formation of sub-200 nm structures on sapphire," CLEO/QELS, May 6-11 (2012) San Jose, CA, USA, Paper CM4E.2.
31. K. Sokolowski-Tinten and D. Von der Linde, "Generation of dense electron-hole plasmas in silicon," Phys. Rev. B **61**, 2643 (2000).
32. R. Le Harzic, D. Dörr, D. Sauer, F. Stracke, and H. Zimmermann, "Generation of high spatial frequency ripples on silicon under ultrashort laser pulses irradiation," Appl. Phys. Lett. **98**, 211905 (2011).
33. M. D. Perry, B. C. Stuart, P. S. Banks, M. D. Feit, V. Yanovsky, and A. M. Rubenchik, Ultrashort-pulse laser machining of dielectric materials, Journal of Applied Physics, 85, (1999).
34. B. C. Stuart, M. D. Feit, S. Herman, A. M. Rubenchik, B. W. Shore, and M. D. Perry, "Nanosecond-to-femtosecond laser-induced breakdown in dielectrics," Phys. Rev. B **53**, 1749 (1996).
35. C. Li, D. Feng, T. Jia, H. Sun, X. Li, S. Xu, X. Wang, and Z. Xu, Solid State Commun., "Ultrafast dynamics in ZnO thin films irradiated by femtosecond lasers," **136**, 389 (2005).
36. J. He, Y. Qu, H. Li, J. Mi, and W. Ji, "Three-photon absorption in ZnO and ZnS crystals," Opt. Express **13**, 9235 (2005).
37. D. Dufft, A. Rosenfeld, S K Das, R. Grunwald, and J. Bonse, "Femtosecond laser-induced periodic surface structures revisited: a comparative study on ZnO," J. Appl. Phys. **105**, 034908 (2009).
38. U. Neumann, R. Grunwald, U. Griebner, G. Steinmeyer, and W. Seeber, "Second harmonic efficiency of ZnO nanolayers," Appl. Phys. Lett. **84**, 170-172 (2004).
39. X. D. Guo, R. X. Li , Y. Hang, Z. Z. Xu, B. K. Yu, H. L. Ma, X. W. Sun, "Raman spectroscopy and luminescent properties of ZnO nanostructures fabricated by femtosecond laser pulses," Mat. Lett. **61**, 4583-4586 (2007).
40. T. Q. Jia, H. X. Chen, M. Huang, F. L. Zhao, J. R. Qiu, R. X. Li, Z. Z. Xu, X. K. He, J. Zhang, and H. Kuroda, "Formation of nanogratings on the surface of a ZnSe crystal irradiated by femtosecond laser pulses," Phys. Rev. B **72**, 125429 (2005).
41. http://www.luxpop.com/
42. A. Borowiec and H. K. Haugen, "Subwavelength ripple formation on the surfaces of compound semiconductors irradiated with femtosecond laser pulses," Appl. Phys. Lett. **82**, 4462-4464 (2003).
43. R. Grunwald, S. K. Das, A. Debroy, E. McGlynn, and H. Messaoudi, "Nonlinear optical mechanism of forming periodical nanostructures in large bandgap dielectrics," in: *IESC Proceedings Series* (Institut d'Études Scientifiques de Cargèse, Corsica, France).

1. Introduction

Laser-induced periodic surface structures (LIPSS), often referred to as ripples, were first reported by Birnbaum in 1965 [1] who found regular micron-scale gratings on laser-irradiated

semiconductor surfaces. From this time, the phenomenon of self-organized structure formation was observed on surfaces of various kinds of solid materials such as metals [2], semiconductors [3,4], dielectrics [5], ceramics [6,7], and polymers [7,8]. The laser-material interaction giving rise to these effects requires laser pulses of appropriate energy, intensity and wavelength and depends on the number of pulses, pulse duration and shape, repetition frequency and the polarization state of the laser field. Taking into account their typical dimensions, two main types of ripples are distinguished in the literature. The first type are the so-called *wavelength ripples* or low spatial frequency LIPSS (LSFL) with spatial periods close to the laser wavelength. To explain the formation of ripple periods near the laser wavelength, a theoretical description on the basis of the excitation of an electromagnetic surface wave interfering with the light field was given by Sipe and co-workers [9]. This model enables an interpretation of the elements of the physical scenario in the very initial stage of the process. In this picture, random scatterers act as dipole like oscillators which are intrinsically sensitive to polarization. The distances between the scatterers are related to a statistical distribution of spatial frequencies providing components which fulfil the *k*-vector dispersion condition for the excitation of the surface plasma wave. The ablation at the points of maximum intensity leads to the amplification of scattering and the increased scattering itself increases the degree of order with increasing numbers of pulses in a positive feedback process. The interference of the surface wave with the incoming light generates a periodically enhanced excitation of the material and the progressive ablation process leads to grating-like structures.

With intense femtosecond laser pulses, however, the appearance of *sub-wavelength ripples* (high spatial frequency LIPSS or HSFL) with significantly smaller spatial periods down to values far below the light wavelength was observed for many kinds of materials. For near infrared femtosecond laser pulses, the period of such structures can be as small as a few tens of nanometers.

By carefully adjusting laser parameters like wavelength, polarization, pulse duration, pulse number or pulse fluence, the shape, size and orientation of the structures created can be controlled, as shown by a range of (mainly empirical) studies [10]. Because this method of structuring is an easy-to-implement, low-cost, top-down method which is able to fabricate periodic structures on the nanoscale without the sophisticated multi-step processes and ultrashort wavelengths needed for nano-lithography, HSFL has gained increasing attraction for practical applications. In particular, emerging fields of nanotechnology and photonics such as surface enhanced Raman spectroscopy (SERS) [11-13], colorization of metals [14,15], incandescent light sources [16], tribology [17], photoelectron emission [18], photovoltaic cells [19], optical memories [20], hydrophobicity control of surfaces [21], and light emitting diodes [22] can benefit from significantly enhanced device efficiencies by the use of this structuring method.

Up to now, the fundamental mechanisms of nanoripple formation are completely understood. Specifically, the different contributions of material transport and self-trapped excitons and plasmons as well as long-term effects like energy deposition or defect accumulation, the influence of second harmonic generation and the relationship between surface and volume structures are still the subject of controversial discussions. Therefore, improved theoretical models are needed to enable a systematic tailoring of the structures, especially if translation to scalable industrial processes is ultimately envisaged. An increasing number of publications indicate the key role of surface plasmon-polaritons (SPPs) in ultrashort-pulse laser induced self-organized nanostructuring. SPPs are a particular kind of surface plasma wave, as described in [9], where light-induced carriers are coupled with the incident radiation field. The analysis of the intrinsic length scales of SPPs [23] in the high-intensity regime, i.e., in the presence of significant nonlinear optical effects, is of considerable practical interest because of its close relationship to the important question of minimum possible feature sizes in nanostructuring.

As we will show in this paper, an extended theoretical model enables us to define conditions for a continuous transfer between LSFL and HSFL and thus to study the material dependent scaling of nanostructure periods as a function of fluence. The excitation of SPPs on metal oxides will be analyzed in detail for the case of ZnO. The results of numerical simulations will be compared to experiments with focused Ti:sapphire laser pulses. The

stability conditions of the different regimes are also considered and limiting factors for the generation of the very highest spatial frequencies are discussed.

2. Surface plasmon-polaritons and ripple periods

Collective charge oscillations at the boundary between an insulating dielectric medium (such as air or glass) and a metal (such as gold, silver or copper) are able to sustain the propagation of infrared or visible SPP-type electromagnetic waves. SPPs are guided along such metal-dielectric interfaces, with the unique characteristics of a sub wavelength-scale confinement perpendicular to the interface. The vector equations governing the resonant excitation of SPPs in a grating structure are

$$\vec{G} = \vec{k}_i - \vec{k}_S \tag{1}$$

$$\Lambda = 2\pi \,|\vec{G}\,|^{-1} \tag{2a}$$

$$\lambda = 2\pi \,|\vec{k}_i\,|^{-1} \tag{2b}$$

$$\lambda_s = 2\pi \,|\vec{k}_S\,|^{-1} \tag{2c}$$

where Λ is the spatial grating period, $\vec{k}_i$ is the wave vector of the incident light, $\vec{k}_S$ is the wave vector for the SPP propagation, λ_s is the wavelength of the SPP, λ is the wavelength of the incident light and $\vec{G}$ is the difference of the *k*-vectors for the incident light and the SPP. From Eqs. (2a)-(2c), for the case of matching the SPP excitation condition, the generated period can be shown to be

$$\Lambda = \frac{\lambda}{\frac{\lambda}{\lambda_s} \pm \sin\theta} \tag{3}$$

where θ is the angle of incidence. At normal incidence ($\theta = 0$), Eq. (3) reduces to the form

$$\Lambda = \lambda_s \tag{4}$$

where the LIPSS period equals the wavelength of the excited SPP. Thus, one way to predict the LIPSS period is to determine the wavelength of the SPP. This SPP wavelength is given by

$$\lambda_s = \lambda \left(\frac{\varepsilon' + \varepsilon_d}{\varepsilon' \varepsilon_d} \right)^{1/2} \tag{5}$$

where λ is the optical wavelength, ε_d is the dielectric function of the insulating medium (here: approximately 1 for air) and ε' is the real part of the dielectric function of the metal (which is < 0). For large bandgap semiconductors and dielectrics, $\varepsilon' > 0$ at optical frequencies and hence the material can not support SPP under linear excitation at low intensities. SPPs can be generated in such materials, however, via efficient multiphoton excitation with ultrashort, intense pulses providing the carriers required to induce a transient metallic state. We propose that the coherently oscillating generated carriers create interference patterns after selecting the resonant spatial frequencies in a polarization-dependent feedback loop driven by scattering, as described in the Sipe model mentioned previously [9] (Fig. 1). Near the ablation threshold, the field enhanced photoelectron emission leaves periodical minima of the electron density (via avalanche ionization) causing a Coulomb explosion of the highly positively charged lattice ions and hence material removal (nonthermal ablation) [24-27].

This hypothesis, of the essential central contribution by SPPs to the ripple formation process, is supported by spectrally and angularly selective experiments with metal gratings [28,29] as well as by the observation of spatial correlations of isolated ripples in sapphire at a fluence close to the ablation threshold [30].

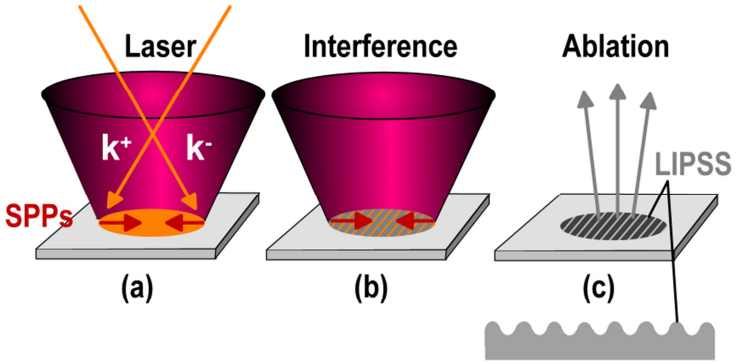

Fig. 1: Schematic diagrams showing the proposed model of the SPP-based process of LIPSS generation: (a) Below-bandgap excitation of a dielectric material via multiphoton absorption of femtosecond laser pulses and coupling of energy into counter-propagating surface plasmon-polaritons (self-organized k-vector matching via Fourier components of random scatterers and feedback according to the Sipe theory [9]), (b) interference of SPPs and light with periods depending on transient index changes, (c) spatially modulated photoelectron generation leads to spatially varying ablation and thus results in grating-like LIPSS structures.

3. Drude model with multiphoton excitation

The below-bandgap excitation of free carriers in transparent dielectric materials is enabled at high intensities where multiphoton absorption dominates and leads to a metal-like behavior. In this case ε' can be written as [26,31]

$$\varepsilon' = \mathrm{Re}\left[\varepsilon - \frac{\omega_p^2}{\omega(\omega + i\Gamma)}\right] \tag{6}$$

where ε is the dielectric function of unexcited material (i.e. without laser induced free electrons), Γ is the electron collision frequency, and ω_p is the plasma frequency. The plasma frequency depends on the carrier density N_c as follows:

$$\omega_p^2 = \frac{e^2 N_c}{m_{eff}\,\varepsilon_0} \tag{7}$$

where m_{eff} is the effective mass of the carriers. If the peak fluence and the order of the absorption process m (which is responsible for the generation of the free carriers) are known, the variation of N_c can also be estimated for dielectrics or insulators. For the generalized case of an absorption process of m^{th} order, N_c can be found by the expression

$$N_c = \frac{\alpha_m F^m (1-R)^m}{m_{eff}\,\pi^{(m-1)/2}\,\hbar\nu\, t_0^{m-1}} \tag{8}$$

where α_m is the m^{th} order absorption coefficient. The validity of the aforementioned generalized equation for the specific cases of m = 1 and 2 can be verified by comparison with earlier reported work [31,32]. It should also be noted that avalanche and Auger recombination processes can affect the carrier density in the general case. However, for the short pulses of

durations ~100 fs used in our experiments, the dominant mechanism controlling the carrier density is multiphoton absorption [33]. Therefore, these other effects were not considered in the model, in order to reduce the computational complexity while maintaining the key physical processes. Furthermore we also note that under excitation conditions consisting of a broadband wavelength spectrum and/or a large angular spectrum (as is typical for focused nJ-range few-cycle laser oscillators), one expects several excitation channels with different values of m to contribute to carrier generation. In case of ZnO (with a bandgap of ~3.4 eV) and a Ti:sapphire laser oscillator with spectral components between 650 nm and 950 nm (corresponding to photon energies between and 1.3 and 1.9 eV) this exponent may have values between m = 2 and m = 3. Under the conditions of an amplified laser with a pulse duration of about 100 fs, used in this work, the bandwidth is < 10 nm and we have taken m = 3. Lastly, we note that in the most general case the carrier density and thus the reflectivity, R, undergo a dynamic evolution, and thus the parameter R in Eq. (8) should vary in time. However, our work uses fluence values close to the damage threshold. In this fluence regime, the critical density is not produced until late in the pulse and thus only the very last part of the laser pulse will experience any strong reflection. In such cases of (close to) damage threshold fluences, the measured and calculated values of R have indeed been found to be low (close to unexcited value) in literature reports, strongly supporting our use of the (constant) unexcited value of the dielectric constant (giving a constant reflectivity value, R = 0.3) in our model. Please refer to Fig. 4 below and the related description by Perry *et al.* in ref. [33]. With these assumptions one can theoretically predict the periods of the ripples on the basis of Eqs. (3)-(8), as will be shown in the following section.

4. Theoretical results

Typical damage thresholds of dielectric materials correspond to values of N_c between 10^{21} and 10^{23}/cm^3 [34]. The variation of the real part of the dielectric function ε' of ZnO for carrier densities between 2 x 10^{21} cm^{-3} and 1.5 x 10^{22} cm^{-3} is shown in Fig. 2.

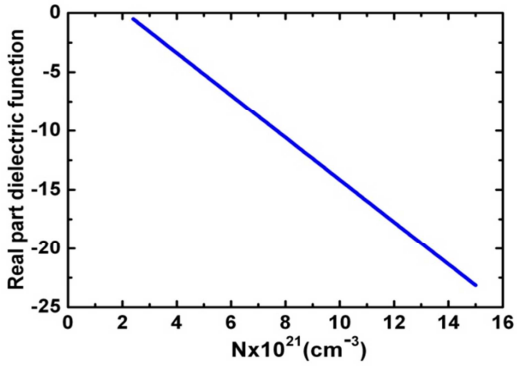

Fig. 2: Real part of the dielectric function of ZnO as a function of the carrier density. The calculation was performed using Eqs. (6) and (7).

The curve was obtained using Eqs. (6) and (7). The values of m_{eff} and Γ for ZnO were assumed to be 0.27 and 1 x 10^{15} Hz, using data from ref. [35]. To enable the existence of SPPs, the real part of the dielectric function must reach negative values. As one can see from Fig. 2, this condition is fulfilled for realistic values of carrier densities. Thus, the initially semiconducting material can temporally turn to a metallic state. This transient metal supports the excitation of SPPs with an oscillation wavelength given by Eq. (5). In the femtosecond laser field, the average carrier density follows the pulse envelope of the pulse. This leads to a fluence-dependent magnitude of the real part of the dielectric function and a varying SPP wavelength (λ_S). The calculated variation of the SPP period with the carrier density according to Eqs. (5)-(7) is plotted in Fig. 3. The different slopes of the curve at low and high carrier densities indicate two distinctly different regions with lower and higher stability corresponding to HSFL and LSFL, respectively. For the HSFL region the slope is very large

indicating a very rapid variation of the the ripple period with the fluence. On the other hand for the LSFL region the slope is negligible indicating a very small variation of the ripple period with the fluence. For practical reasons it is useful to express this dependence in terms of the laser fluence instead of the carrier density because this enables a direct comparison of our theoretical predictions and experimental findings. The relationship of carrier density to fluence for ZnO assuming a three-photon absorption (m = 3) and a FWHM pulse duration of t_0 = 130 fs is shown in Fig. 4. In accordance with data in the literature, the value of α_3 was taken to be 0.01 cm^3/GW^2 [36].

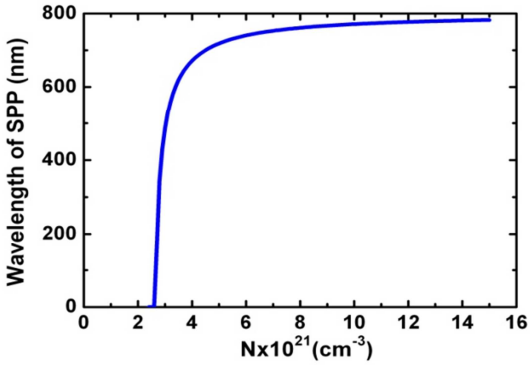

Fig. 3: Theoretically predicted SPP wavelength of ZnO as a function of the carrier density. The calculation was performed using Eqs. (5)-(7).

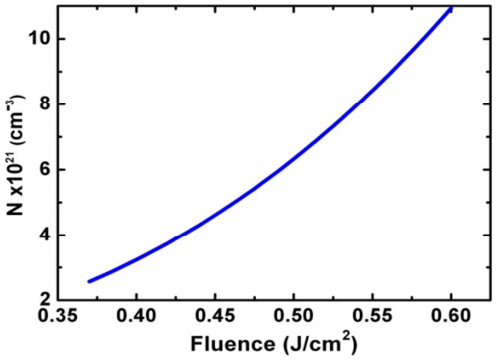

Fig. 4: Variation of the carrier density with the fluence for ZnO using Eq. (10).

The value of fluence variation was assumed to be 0.37-0.6 J/cm^2 corresponding to the fluence interval for which a distinct LIPSS formation was experimentally demonstrated on ZnO with femtosecond pulses at 800 nm [37]. Fig. 4 confirms the range of N_c for material damage consistent with reports in the literature [36]. The corresponding theoretical fluence dependencies of ε' and λ_S are shown in Figs. 5 and 6, respectively.

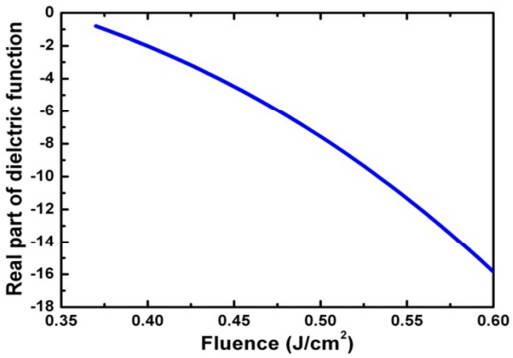

Fig. 5: Theoretically predicted variation of the real part ε' of the dielectric function with increasing fluence for ZnO.

In conjunction with Fig. 2, the data in Fig. 5 gives direct evidence of the feasibility of achieving negative values of ε' due to the excitation of the material in the fluence region where the ripple formation is obtained in the case of ZnO.

The theoretically simulated physical content in Fig. 6 (solid line) is identical with that shown in Fig. 3. The fluence-dependent predicted SPP periods, however, can be directly compared to the experimentally measured nanostructure periods. Two extreme cases, for small and high fluence values, appear which correspond to the HSFL and LSFL, respectively. Furthermore, the stability (i.e. the dependence on small fluctuations of the fluence or other distortions) is significantly different for both regions. Specifically we note that, the transition between the extreme cases predicted by this theory is continuous (and does not display a bifurcation).

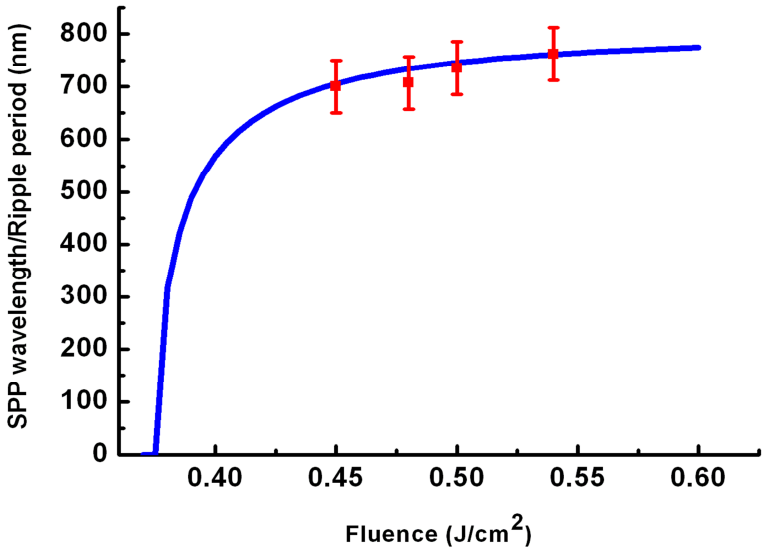

Fig. 6: Variation of the SPP wavelength as a function of fluence for ZnO (blue solid curve). Two distinct regions can be identified which correspond to HSFL and LSFL. The transition between HSFL and LSFL regions is continuous. The red squares and error bars correspond to experimental data and are discussed in section 5.

5. Experimental results

In order to verify the theoretical predictions above, LIPSS formation on crystalline bulk ZnO

(hydrothermally grown crystals, obtained from Tokyo Denpa Ltd and Crystal GmbH) were studied with an amplified Ti:sapphire laser system delivering linearly polarized pulses with a duration of 130 fs at a central wavelength of 800 nm and a spectral FWHM bandwidth of < 10 nm. Two sets of experiments were performed with tightly and loosely focused beams ($1/e^2$ waists: 16 and 66 µm, respectively) at approximately normal incidence (maximum incident angle: < 2°). To ensure the data comparability, all experiments were done with equal pulse numbers (N = 10). The nanostructures were characterized with a field-emission scanning electron microscope (FE-SEM; JEOL JSM 64-00F). Because of the spatial variation of the laser intensity, the spatial frequency spectrum had to be analyzed in a locally resolved manner. To improve the accuracy, in some cases (e.g. data in Fig. 6), we compared two methods: (a) a Fourier analysis of small sections, and (b) averaged local profiles. The agreement between both analyses was very good (within a few percent). The ZnO crystal surface termination was *c*-plane (i.e., with a minimum second harmonic generation efficiency at normal incidence [38] in contrast to *a*-plane material).

From the experiment set #1, the LSFL periods at the centers of the laser irradiated spots were determined from SEM images, as shown in Figs. 7a-d. The experimental results shown in Fig 6 as the scattered points, were found to agree well with the theoretically estimated SPP wavelengths. Furthermore, it is important to note that (as predicted by the theory) the periods were found to be quite insensitive to the intensity in the LSFL regime.

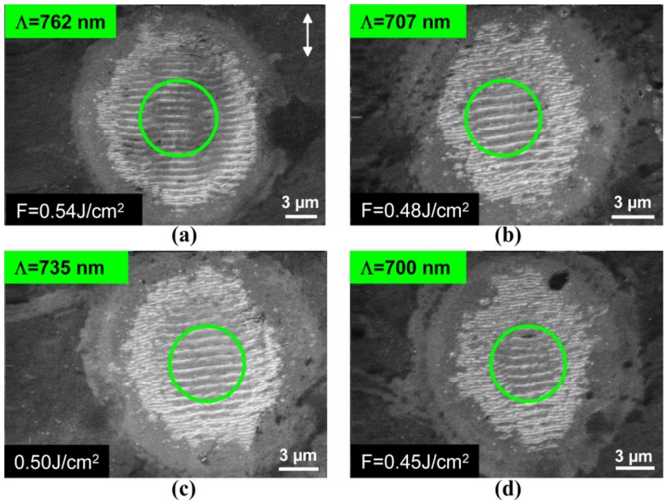

Fig. 7: Scanning electron microscope (SEM) images of LIPSS on ZnO obtained at different peak fluences of a Ti:sapphire laser, (a) 0.54 J/cm^2, (b) 0.50 J/cm^2, (c) 0.48 J/cm^2, (d) 0.45 J/cm^2 (pulse duration 130 fs, center wavelength 800 nm, LIPSS direction perpendicular to the polarization vector which is indicated by the white double arrow). The LSFL periods plotted as data points in Fig. 6 were determined from the regions at the centers of the green circles.

From the theoretical curve in Fig. 6 one has to expect that in the relevant parameter range the period of ripples varies continuously with the intensity. Experimental data in this range suffers from large errors because of the high sensitivity of this parameter to small fluence variations (the derivation of SPP period of the fluence rises steeply toward the left part of the curve in Fig. 6). Therefore, the continuous and rapid transition to HSFL is demonstrated by experiment set#2, exploiting the spatially variable fluence profile at the rim of the focused Gaussian beam (Fig. 8). The blue solid line in this figure demonstrates the theoretical variation of the SPP wavelength as calculated from the spatially varying intensity profile of the Gaussian beam. Excellent agreement was found, except at very small fluence values at the edges of the spot. Once again in the LSFL region the SPP period is oberved to be quite insensitive to the fluence over a ~ 10 µm range, while a very fast variation in SPP period was seen in the HSFL region of a width ~ 4 µm. This striking radial dependence of the period gives further compelling evidence in favour of the SPP based model of the LIPSS formation

mechanism proposed above. It is also noteworthy to point out that, in contrast to our model, theories explaining LIPSS formation based on second harmonic generation (SHG) predict that the smallest period of subwavelength ripples should be equal to $\lambda_F/2n_{SHG}$ [40] where λ_F and n_{SHG} are the wavelength of the fundamental and the refractive index of the SHG contribution, respectively.

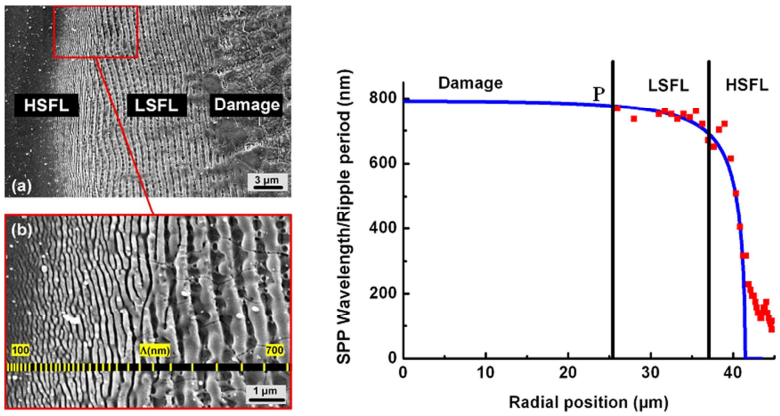

Fig. 8: (a) and (b): SEM images showing the continuous transition from LSFL to HSFL for a spatially varying fluence profile (with a Gaussian beam focus), towards the edge of the laser spot region. The image in (a) contains a damaged area corresponding to the highest fluence (> 0.82 J/cm^2, right), an extended area with slowly varying LSFL (center) at medium fluence and HSFL in the low-fluence outer part. The image in (b) below shows an enlarged section of (a) measured at higher SEM resolution. The fluence varies between 0.6 J/cm^2 (right side) and about 0.37 J/cm^2 (left side). Despite some randomness, the radial variation of the period can clearly be recognized (indicated by the yellow lines in the horizontal black bar). The largest periods were measured to be about 720 nm, whereas the smallest periods are around 100 nm (with some variation in this region). The change of period from the center towards the rim of the laser spot is shown in (c), with indications given of specific regions also shown in (a), and the theoretical prediction is given by the solid blue line.

In [40] this was verified for SiC periods down to 90 nm. Our theoretical results, however, indicate that ripple periods in semiconductors or dielectrics can reach significantly smaller values than $\lambda_F/2n_{SHG}$. This agrees with experimental results on graphite and diamond as published by other groups [25]. The smallest periods experimentally observed on ZnO in this work are about 100 nm (in the rim zone of Fig. 9). This value is much smaller than the value of $\lambda_F/2n_{SHG}$ which is about 177 nm (λ_F = 800 nm and n_{SHG} = 2.26 [41]). Furthermore, in contrast to the experiments reported in [40], no rotation of the LSFL relative to the HSFL is observed under the conditions of the experiments reported here. Concerning the rotation of ripple orientation we believe that the SHG (which, as we think, cannot be the only factor) must play a significant role under certain circumstances, specifically concerning different competing plasmon modes. This topic is currently the subject of further studies.

Finally we like to note that experiments were also performed with other materials like Al_2O_3. The intensity dependence behaviour of LIPSS in this material was found to be similar to the results we have reported above for ZnO. Borowiec et al. [42] reported on the generation of both HSFL and LSFL in their experiments with Al_2O_3. They qualitatively attributed the origin of HSFL in this as well as other large bandgap materials to a multiphoton excitation of carriers. Our quantitative model strongly supports this hypothesis.

6. Conclusions

To conclude, the SPP-based origin of sub-wavelength ripples on dielectrics and semiconductors like ZnO after irradiation with near infrared femtosecond pulses was confirmed, based on the excellent agreement of a theoretical model describing this mechanism with our experimental data. The results of simulations and experiments indicate that the

generation of SPPs plays a major role in the mechanism of LIPSS formation. Multiphoton absorption enables a below-bandgap excitation of free carriers and switches the real part of the dielectric function temporally to negative values.

For the first time it has been demonstrated that, in the fluence range near the damage threshold for femtosecond-laser excitation, a dielectric material can indeed satisfy the excitation condition for SPPs. It was shown that the spatial frequencies of the plasmons which directly determine the ripple periods are a function of the fluence-dependent density of free carriers. At high fluence, the plasmon wavelength approximates the optical wavelength in a stable regime, whereas very small periods and high instability are characteristic of the low fluence regime [43]. The predicted behavior agrees well with the experimental findings. In the low-fluence regime, we observed HSFL periods down to 1/8 of the wavelength.

The present simulation, using the idealized situation of a time-averaged model, actually predicts the formation of SPP periods down to a theoretical value of zero at $\varepsilon' = -1$ corresponding to arbitrarily small periods. However, the reduced efficiency of multiphoton excitation towards lower fluence, fluctuations in the laser parameters, the ablation threshold and the structural features of the material such as roughness are limiting factors for the smallest possible periods in real experiments.

Future studies will needed to extend the theoretical approach to a *time-dependent* Drude theory. These studies will need to the additional consideration that the time dependent carrier density generates a time-variant SPP period which is averaged over the pulse during the period above the ablation threshold. The possible contribution of a two-photon induced bandgap shrinking is still under discussion and requires highly selective experiments in the time domain. In the calculations this effect could lead to a smaller effective nonlinear exponent. The influence of previously existing ripples on the SPP dynamics with increasing pulse numbers is also an interesting open question.

ACKNOWLEDGEMENTS

The authors thank T. Elsaesser, R. Mueller, K. Busch, A. Rosenfeld and S. Kühn (MBI), P. Kazansky (ORC, Southampton), Y. Bellouard (University Eindhoven), W. Seeber (Otto Schott Institute Jena), Y. Cheng (Shanghai Institute of Optics and Fine Mechanics), R. Stoian, S. Sakabe (Kyoto University), J. Reif (TU Cottbus), J. Bonse (BAM Berlin) and F. Güell (University Barcelona) for stimulating discussions, and M. Tischer (MBI) for analysis of the nanostructures using scanning electron microscopy. The work was supported by DFG and LaserLab Europe under grant numbers GR 1782/12-2 and MBI 001663, respectively and Enda McGlynn is particularly grateful for LaserLab Europe and MBI support and hospitality during visits to MBI. Abishek Debroy was involved for two months and was supported during this period by the 2012 WISE Programme of the DAAD.